

# Quantum phases of ferromagnetically coupled dimers on Shastry-Sutherland lattice

Monalisa Chatterjee,<sup>\*</sup> Santanu Pal,<sup>†</sup> and Manoranjan Kumar<sup>‡</sup>

*S. N. Bose National Centre for Basic Sciences, Block-JD, Sector-III, Salt Lake, Kolkata 700106, India*

The ground state (gs) of antiferromagnetically coupled dimers on the Shastry-Sutherland lattice (SSL) stabilizes many exotic phases and has been extensively studied. The gs properties of ferromagnetically coupled dimers on SSL are equally important but unexplored. In this model the exchange coupling along the  $x$ -axis ( $J_x$ ) and  $y$ -axis ( $J_y$ ) are ferromagnetic and the diagonal exchange coupling ( $J$ ) is antiferromagnetic. In this work we explore the quantum phase diagram of ferromagnetically coupled dimer model numerically using density matrix renormalization group (DMRG) method. We note that in  $J_x$ - $J_y$  parameter space this model exhibits six interesting phases: (I) stripe  $(0, \pi)$ , (II) stripe  $(\pi, 0)$ , (III) perfect dimer, (IV)  $X$ -spiral, (V)  $Y$ -spiral and (VI) ferromagnetic phase. Phase boundaries of these quantum phases are determined using the correlation functions and gs energies. We also notice the correlation length in this system is less than four lattice units in most of the parameter regimes. The non-collinear behaviour in  $X$ -spiral and  $Y$ -spiral phase and the dependence of pitch angles on model parameters are also studied.

## I. INTRODUCTION

Frustrated magnetic systems are promising materials to explore exotic phases like dimer<sup>1</sup>, non-collinear spin wave<sup>2</sup>, spin-liquid<sup>3,4</sup>, non-trivial topological phase<sup>5-8</sup> in the ground state (gs). In the last couple of decades these systems are extensively synthesized in various dimensions for example, in one dimensional geometry: LiCuSbO<sub>4</sub><sup>9</sup>, LiCuVO<sub>4</sub><sup>10</sup> and Rb<sub>2</sub>Cu<sub>2</sub>Mo<sub>3</sub>O<sub>12</sub><sup>11,12</sup>; in ladder like geometry: SrCu<sub>2</sub>O<sub>3</sub><sup>13</sup> and (VO)<sub>2</sub>P<sub>2</sub>O<sub>7</sub><sup>14,15</sup>; in two dimensional systems such as ZnCu<sub>3</sub>(OH)<sub>6</sub>Cl<sub>2</sub> (Herbertsmithite)<sup>7,16,17</sup> and  $\alpha$ -RuCl<sub>3</sub><sup>18</sup>. Their properties have been rigorously explored theoretically as well<sup>19-22</sup>. In presence of a finite magnetic field, these systems exhibit plethora of quantum phases like multipolar<sup>23</sup>, spin nematic<sup>24</sup>, vector chiral<sup>25</sup>, plateaus state at various fractional magnetization<sup>5,6,26-28</sup>. To explain the physical properties of these systems various models have been proposed like Heisenberg spin-1/2  $J_1$ - $J_2$  model for one dimensional (1D) spin chain<sup>1,29-31</sup>, Heisenberg anti-ferromagnetic spin-1/2 model on Shastry-Sutherland lattice (SSL)<sup>32</sup> and square lattice<sup>33</sup>,  $J_1$ - $J_2$  model on square lattice<sup>34,35</sup> etc.

In general, frustrated 2D magnets are found in layered materials<sup>36</sup> and these 2D geometries: square<sup>37</sup>, triangular<sup>38</sup>, kagome<sup>17</sup> and SSL<sup>39-41</sup> are particularly interesting because 2D is supposed to be a critical dimension in the purview of Mermin-Wagner theorem<sup>42</sup>. We are particularly interested in SSL which is shown in Fig. 1. This structure is similar to a square lattice except alternate squares have a diagonal bond. If a isotropic Heisenberg spin-1/2 model on the SSL is considered with antiferromagnetic exchange along the square  $J_x = J_y$  and diagonal exchange  $J = 2J_x = 2J_y$  then the model can be solved exactly<sup>32</sup>. The ground state of this system has Néel and dimer order for small and large  $J/J_y$  limit respectively considering ( $J_x = J_y$ ). Corboz *et al.*<sup>43</sup> predicted the existence of a plaquette phase between Néel and dimer region using the PEPS technique, whereas,

very recently, Yang *et al.*<sup>44</sup> predicted a spin liquid phase. While it's exact nature has been controversial, Ronquillo and Peterson<sup>45</sup> predicted the topological gs.

Among the layered magnetic materials, spin-1/2 layered copper oxyhalides (CuX) <sub>$A_{n-1}$</sub> B <sub>$n$</sub> O <sub>$3n+1$</sub>  are frustrated 2D magnets which have many interesting features just by tuning the composition. The CuX layers are sandwiched by non-magnetic layers, the anion orbitals are involved in exchange pathways but the cation orbitals replacement keeps the magnetic layer homogeneous. However, a small change in exchange interaction can be tuned by changing the lattice parameters, electrostatic fields, and crystal-field splittings<sup>46</sup>. The tuning of anion and cation composition can drive the system across the quantum critical points. Experimental results suggest that the gs can be tuned to have a collective singlet with a spin gap in (CuCl)LaNb<sub>2</sub>O<sub>7</sub>,<sup>47-50</sup>, a collinear stripe magnetic order in (CuBr)LaNb<sub>2</sub>O<sub>7</sub>,<sup>51</sup> and a magnetization plateau at 1/3 of the saturated moment in (CuBr)Sr<sub>2</sub>Nb<sub>3</sub>O<sub>10</sub><sup>52</sup>.

(CuCl)LaNb<sub>2</sub>O<sub>7</sub> was initially predicted as  $S = 1/2$  frustrated square lattice<sup>47</sup>, however, band structure calculations revealed that the simplest model for this material can be best described as strong antiferromagnetic (AFM) exchange interaction between fourth neighbours forming a strong singlet dimer and these dimers are coupled together by ferromagnetic (FM) interactions i.e this model looks like the Shastry-Sutherland model with ferromagnetic exchange  $J_x$  and  $J_y$  along square and antiferromagnetic diagonal exchange  $J$ <sup>53</sup>. This model was theoretically studied using mean-field and exact diagonalization (ED) methods on a small cluster and they predicated a plethora of phases in exchange parameter space<sup>54</sup>. In the intermediate FM coupling limit, they reported two types of stripe phases,  $(0, \pi)$  and  $(\pi, 0)$ , separated by a non-collinear spiral phase. The dimer singlet stabilizes for  $J_x, J_y < J/2$ , whereas ferromagnetic gs is stable for large  $J_x$  and  $J_y$ <sup>54</sup>. We notice that the phase boundaries as well as the existence of different phases calculated from ED are not consistent with that calculated from mean-field, for example, non-collinear phase does not appear in exact diagonalization results, but is

present in the mean field calculations. Therefore, it is very intriguing to explore such an interesting model with a more sophisticated numerical tool like density matrix renormalization group (DMRG) method which can give accurate results for large lattice sizes.

In this work, we explore the ferromagnetically coupled  $S = 1/2$  dimers on SSL with the DMRG method and re-investigate the quantum phase diagram of this model. The phase diagram is based on the nature of spin-spin correlations and ground state energy variation. The gs exhibits predominantly six types of phases: two types of stripe order with wave vector  $(0, \pi)$  and  $(\pi, 0)$  for large value  $J_y$  and  $J_x$  respectively. A perfect dimer phase exists for  $J_x = J_y$  and this phase separates two types of spiral phases namely  $X$ -spiral with wave vector  $(\theta, 0)$  and  $Y$ -spiral with wavevector  $(0, \theta)$ , where  $\theta$  is the pitch angle. In the large limit of  $J_x$  and  $J_y$  the gs has ferromagnetic behaviour. We also explore the effect of  $J_x$  and  $J_y$  on spiral behaviour and pitch angle and we notice that spin ordering is very short range in most of the parameter regimes.

The paper is organized as follows. In Sec. II, the model of the ferromagnetically coupled SSL and numerical methods are discussed. In Sec. III, all the numerical results are presented and this section has four subsections. The quantum phase diagram is presented in Sec. III A. Sec. III B and Sec. III C discuss gs energy and spin-spin correlation in various phases of the phase diagram. The pitch angles are discussed in Sec. III D. Results are discussed and compared with literature in Sec. IV. In an appendix we presented results for the ground state energy per site and spin-spin correlation for various bond dimensions ( $m$ ) and various system sizes.

## II. MODEL HAMILTONIAN AND NUMERICAL METHODS

We consider a Heisenberg spin  $S = 1/2$  model on SSL where only diagonal interaction  $J = 1$  is antiferromagnet and sets the energy scale of the system. The strength of ferromagnetic exchange interaction along the  $x$ -axis and  $y$ -axis on the square is represented by  $J_x$  and  $J_y$  respectively. The arrangement of the exchange interactions are shown in Fig. 1. Now onward we will call this model as Shastry-Sutherland (SSM) and can be written as

$$H = -J_x \sum_{\langle ij \rangle_x} \vec{S}_i \cdot \vec{S}_j - J_y \sum_{\langle ij \rangle_y} \vec{S}_i \cdot \vec{S}_j + J \sum_{\langle ij \rangle_d} \vec{S}_i \cdot \vec{S}_j \quad (1)$$

where the first sum runs for NN bonds along the  $x$ -direction, the second sum runs for NN bonds along the  $y$ -direction and the last sum runs for NN diagonal bonds in the square.

We use the exact diagonalization for system size up to 32 sites and the density matrix renormalization group (DMRG) method<sup>55–58</sup> for large system size. The DMRG method is a state of art numerical method to handle the large degrees of freedom for a many-body Hamiltonian

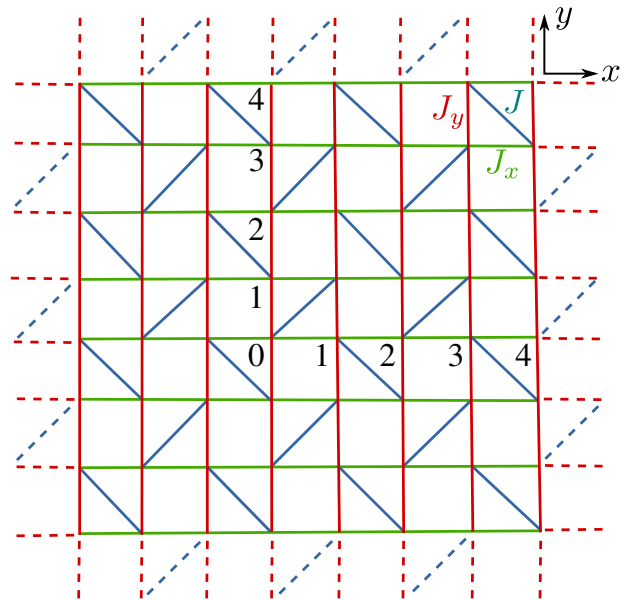


FIG. 1. Figure shows a schematic diagram of SSL. The coupling constants along  $x$ -axis ( $J_x$ ) and along  $y$ -axis ( $J_y$ ) are FM and the diagonal bond couplings  $J$  are AFM in nature. The site index 0 is the reference site and the numbers along  $x$ -axis and  $y$ -axis represent the distance ( $r$ ) from the reference site.

in low dimensions. This method is based on the systematic truncation of irrelevant degrees of freedom while growing the system sizes and optimising the wavefunction while doing the finite DMRG algorithm. In this work, we use a modified DMRG method<sup>59</sup> in which 4-new sites are added at each step to reduce the number of times of renormalization of operators used to build the super block<sup>59</sup>. We retain up to  $m = 900$  block states which are the eigenvectors of the system block density matrix corresponding to the largest eigenvalues. The chosen value of ' $m$ ' keeps the truncation error to less than  $\sim 10^{-8}$ . We also carry out 10 – 12 finite sweeps for improved convergence and to optimise the wave function. We use cylindrical geometry of the SSL and a periodic boundary is applied along the width of the lattice and open boundary along the length. The largest system size studied is up to  $12 \times 8$  (length  $\times$  width) system size. We have analysed the convergence of energy with the various values of  $m$  in appendix. The per-site energies for  $12 \times 4$  system are shown for  $m = 256, 512$  and  $900$ , whereas for  $12 \times 8$  system, it is shown for  $m = 256, 512$  and  $700$  in table I. We notice that  $m = 512$  is sufficient for accuracy up to 5<sup>th</sup> decimal place for  $12 \times 4$  and 4<sup>th</sup> for  $12 \times 8$  system. We also show the dependence of the spin-spin correlation function on  $m$  in table II and III of appendix. We notice that the spin-spin correlations are accurate up to 4<sup>th</sup> decimal places. Interestingly this model gives amazing accuracy of energies as well as correlation function and these accuracy may be attributed to the short-range

correlation length which is approximately 4 lattice unit.

### III. RESULTS

To identify the existence of various phases of the model with isotropic Heisenberg exchange in Eq. 1, we calculate spin-spin correlation  $C(r)$  and gs energies. There are six different phases in this model: (i) stripe  $(0, \pi)$  where the spin configuration has a propagation vector  $(k_x, k_y) = (0, \pi)$  and the system forms stripes along the  $x$ -direction where all the spins along  $x$ -direction are arranged ferromagnetically while spin modulates with wavevector  $\pi$  along the  $y$ -direction as shown in Fig. 2(a). (ii) In the stripe  $(\pi, 0)$  phase, stripes run along the  $y$ -direction where spins are arranged ferromagnetically in  $y$ -direction while spin wave has wavevector  $\pi$  along the  $x$ -direction as shown in Fig. 2(b). (iii) The ground state with a  $X$ -spiral phase has a non-collinear arrangement of spins along the  $x$ -direction and ferromagnetic ordering along the  $y$ -direction as shown in Fig. 2(c). This phase appears in case of highly frustrated model with AFM  $J_x = J_y$  in Ref. [32]. (iv) In  $Y$ -spiral phase, spins have a non-collinear arrangements along the  $y$ -direction and ferromagnetic ordering sets in along  $x$ -direction as in Fig. 2(d). (v) In the perfect dimer phase the gs wave function can be represented as a product of dimer singlets:  $|\psi\rangle \equiv \prod_d \frac{1}{\sqrt{2}}(|\uparrow\downarrow\rangle - |\downarrow\uparrow\rangle)_d$ , where  $d$  labels a dimer<sup>32,54</sup>. In this phase, the dimers are formed along the diagonal bonds as shown in Fig. 2 (e). The spin-spin correlation  $C(r) = -0.75$  along the diagonal bonds and  $C(r) = 0$  along any other bonds on the square. (vi) When the FM couplings dominate over the diagonal antiferromagnetic exchange interaction the FM phase appears. In this phase, all spins are aligned in the same direction as shown in Fig. 2(f).

#### A. Quantum Phase Diagram

In this section, the quantum phase diagram is presented in  $J_x$  and  $J_y$  parameter space as shown in Fig.3 for a given diagonal exchange  $J = 1$ . For a large value of  $J_x$  or  $J_y$  stripe phases with wave vectors  $(0, \pi)$  and  $(\pi, 0)$  stabilized in the gs of the system. In this region, frustration is considerably small due to the small or large value of  $J_x/J_y$ . The strong FM coupling bonds prefer FM spin orderings, whereas, weak FM coupling bonds prefer antiferromagnetic spin ordering to satisfy the diagonal AFM exchange. For the moderate exchange strength  $J_x < 1$  and  $J_y < 1$  the gs has non-collinear spin ordering. Depending on the relative exchange strength of  $J_x$  and  $J_y$  there are two types of spiral phases:  $X$ -spiral and  $Y$ -spiral. These two spiral phases are separated by a perfect dimer phase formed along the line  $J_x = J_y$  and extended up to  $J_x, J_y \lesssim J$ . The perfect dimer region is confined along the  $J_x = J_y$  line as  $C(r = 2)$  continuously increases

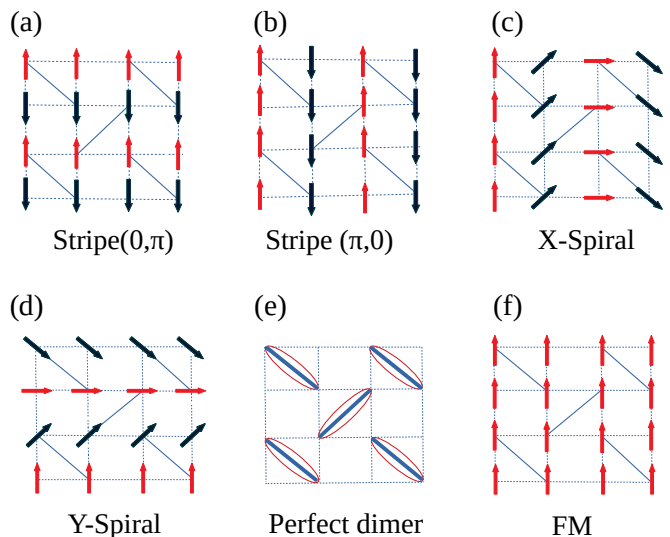


FIG. 2. Figure shows a schematic diagram of different phases present in the ferromagnetically coupled dimers on the SSL, where arrows represent the spin alignments and the ellipses are the dimers (defined in the main text). (a) and (b) are two stripe phases with ordering wave vector  $(0, \pi)$  and  $(\pi, 0)$  respectively. (c) and (d) are two non-collinear spiral phases, the  $X$ -spiral and  $Y$ -spiral. (e) and (f) are the perfect dimer and FM phase respectively.

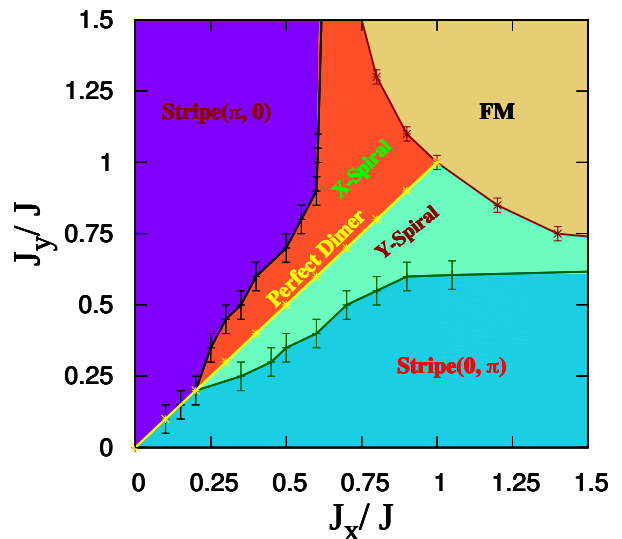


FIG. 3. Figure shows the quantum phase diagram of the SSM. The phase diagram comprises six phases: Two stripe order phases with ordering wave vector  $(0, \pi)$  and  $(\pi, 0)$ , two spiral orders along both the  $x$ - and  $y$ -directions, the  $X$ -spiral and  $Y$ -spiral phase respectively. The other two phases are a perfect dimer phase (the yellow line separating two spiral phases) and a phase with FM spin ordering along all directions of the lattice.

with  $|J_x - J_y|$ . In the strong coupling region of  $J_x$  and  $J_y$ , long-range FM magnetic ordering sets in.

## B. Ground state energy

Ground state energies are calculated for the model in Eq. 1 on a cylindrical geometry with periodic boundary condition (PBC) along the width ( $y$ -axis) and open boundary condition along the length ( $x$ -axis), and  $12 \times 4$  system is used to calculate the accurate gs. In Fig. 4 the gs energy per site  $\epsilon_{gs}$  is plotted as a function of  $J_y$  by keeping  $J_x$  fixed value of  $J_x = 0.9$ . Around  $J_y \sim 1.1$  we saw a discontinuity in the gs energy, indicating a first-order phase transition from FM to  $X$ -spiral phase. The maxima of the energy curve is close to  $J_x = J_y \sim 0.9$  which indicates the dimer line, and the small deviation of maxima from dimer line  $J_x = J_y$  is due to the rectangular geometry of the lattice. The maxima shifts to  $J_x = J_y$  line as we increase the width of the lattice. The smooth variation of  $\epsilon_{gs}$  with  $J_y$  indicates the second-order dimer transition. No signature of spiral and stripe transitions is detected from the gs energy variation.

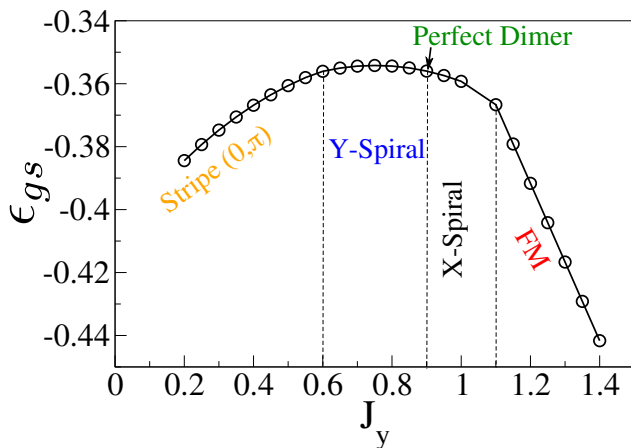


FIG. 4. Figure shows gs energy per site ( $\epsilon_{gs}$ ) versus  $J_y$  plot at  $J_x = 0.9$  for  $12 \times 4$  lattice sites of the SSM. Around  $J_y = 1.1$  we show a kink in the energy curve indicating a sharp phase transition from  $X$ -spiral to FM phase. The transition between the two spiral phases is not sharp. Around  $J_y = 0.6$  system transits from  $Y$ -spiral to stripe  $(0, \pi)$  phase. (Shaded lines are only for eye guide of the transition points).

## C. Spin-spin correlation

In this subsection, we present spin-spin correlation  $C(r)$  for various parameter regimes to validate the existence of different phases in the phase diagram in Fig. 3. We are dealing with isotropic system and total spin-spin correlations  $C(r) = \langle \vec{S}_i \cdot \vec{S}_{i+r} \rangle = 3 \langle S_i^z S_{i+r}^z \rangle$  where  $S_i^z$  represents the  $z$ -component of the spin operator at the reference site  $i$ .  $r$  is the distance between the spin site and reference site along the  $x$ - and  $y$ -axis as shown in Fig. 1. The spin Hamiltonian in Eq. 1 has  $SU(2)$  symmetry and one expects equal spin-spin correlation for all three

spin components in the singlet sector. To understand the spin arrangements in different phases we have calculated  $C(r)$  along different spatial directions. In Fig. 1, the site with 0 index represents the reference site, from which correlations are calculated in various directions, and distances  $r$  are shown in various directions with numerals as shown in Fig. 1. In Fig. 5(a) we presented  $C(r)$  along

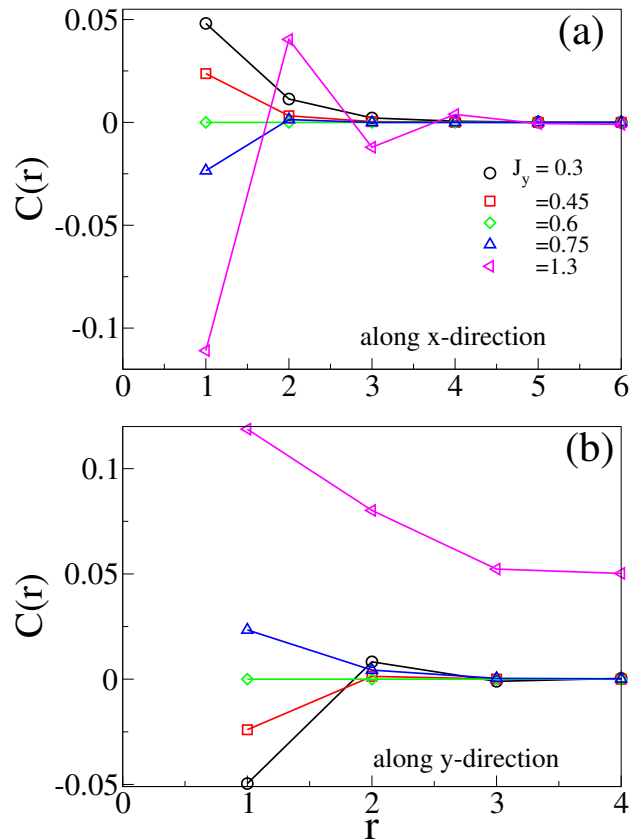


FIG. 5. Figure shows the variation of spin-spin correlations  $C(r)$  with distance ( $r$ ) for  $12 \times 8$  system size. Spin-spin correlations are calculated for different  $J_y$  values by keeping  $J_x$  fixed at 0.6. (a)  $C(r)$  are calculated along  $x$ -direction. (b)  $C(r)$  are calculated along  $y$ -direction.

the  $x$ -direction, whereas Fig. 5 (b) represents the same for  $y$ -direction. In all plots, we have fixed  $J_x = 0.6$  and calculated  $C(r)$  for different  $J_y = 0.3, 0.45, 0.6, 0.75$  and  $1.3$ , where  $J_y$  values correspond to different phases in the phase diagram.

In Fig. 5(a) for  $J_y = 0.3$ , all the values of  $C(r)$  are positive which correspond to an FM spin arrangement along  $x$ -direction. Whereas in Fig. 5(b) for same value of  $J_y = 0.3$ ,  $C(r)$  shows an antiferromagnetic arrangement of spins along  $y$ -direction. This kind of spin arrangements correspond to a stripe spin ordering with a wave vector  $(0, \pi)$  (see Fig.2(a)). For  $J_y = 1.3$  the behaviour of the spin correlation along the  $x$ -direction interchanges with the behaviour along  $y$ -direction i.e antiferromagnetic arrangement along the  $x$ -direction and ferromagnetic ar-

rangement along the  $y$ -direction. This represents another kind of stripe phase with wave vector at  $(\pi, 0)$  as shown in Fig. 2(b).

At  $J_y = 0.45$ ,  $C(r)$  along  $x$ -direction are all positive and correspond to an FM spin alignment in this direction, whereas in the  $y$ -direction the  $C(r)$  is non-collinear i.e pitch angle is different from 0 or  $\pi$ . The non-collinear spin arrangement is shown along the  $y$ -direction and the Y-spiral phase can be seen in Fig. 2(d). For  $J_y = 0.75$ ,  $C(r)$  shows a non-collinear behaviour along  $x$ -direction whereas ferromagnetic behaviour along the  $y$ -direction. The schematic of X-spiral phase is shown in Fig. 2(c).

When  $J_x = J_y (= 0.6)$ ,  $C(r)$  along  $x$ -direction and  $y$ -direction are exactly zero, whereas, we found the correlation for diagonal bonds are  $-0.75$ . This shows a perfect dimer formation along the diagonal bonds and this phase is shown in Fig. 2(e). A perfect dimer phase is formed along  $J_x = J_y \lesssim 1$  line. In low  $J_x$  and  $J_y$  limit  $C(r > 1)$  have non zero value for  $|J_x - J_y| > 0$ , therefore the perfect dimer phase is only restricted to  $J_x = J_y$ . In the FM phase region  $C(r)$  have all positive values in all directions.

#### D. Pitch angle

In a geometrically frustrated system wavevector or the pitch angle of a non-collinear spin ordering, in general, depends on the competing exchange interactions<sup>60–62</sup> and therefore, it is important to understand behaviour of pitch angle  $\theta$  in various exchange interaction limits to quantify spin modulation in terms of the pitch angle  $Q_x$  and  $Q_y$ . Fig. 6(a) shows spin-spin correlation  $C(r)$  for  $J_x = 0.7$  for different  $J_y$  values inside the X-spiral region.  $C(r)$  shows the exponentially decaying behaviour with distance  $r$ . It indicates the non-collinear spin ordering along  $x$ -direction, representing the X-spiral phase.  $C(r)$  in Fig. 6(a) shows an exponential decay, representing a very short-range correlation in the spiral region. Pitch angle ( $Q_x$ ) can be calculated in the X-spiral phase, by fitting  $C(r)$  with the following equation

$$C(r) = a_0 \cos(Q_x r + c) e^{-\frac{r}{\xi}}, \quad (2)$$

where  $\xi$  is the correlation length,  $a_0$  and  $c$  are constants. To calculate the pitch angles in the Y-spiral phase, a similar correlation function can be applied as above, where  $Q_x$  will be replaced by  $Q_y$ . The variation of pitch angle  $Q_x$  with  $J_y$  is presented in Fig. 6(b) and we notice that  $Q_x$  varies between 0 to  $\pi$ . We also notice that  $Q_x$  changes sharply near  $J_x \sim 0.6$ .  $Q_x$  and  $Q_y$  variation with  $J_y$  and  $J_x$  for a classical system<sup>54</sup> can be given as

$$\begin{aligned} \cos(Q_x) &= -\frac{J_y}{J} + \frac{J}{4J_x} \left( \frac{J_y}{J_x} - \frac{J_x}{J_y} \right), \\ \cos(Q_y) &= -\frac{J_x}{J} + \frac{J}{4J_y} \left( \frac{J_x}{J_y} - \frac{J_y}{J_x} \right). \end{aligned} \quad (3)$$

The classical results seem to deviate significantly from our calculated values. The DMRG results are shown as

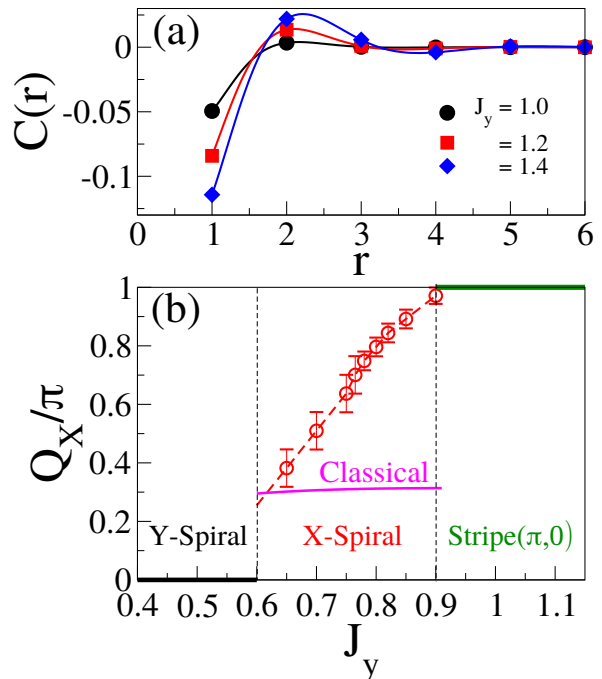


FIG. 6. Figure (a) shows the spin-spin correlation  $C(r)$  along length ( $x$ -direction) for different  $J_y$  at  $J_x = 0.7$ . The solid curves represent respective fits with exponentially decaying function. In figure (b) we have plotted pitch angle ( $Q_x/\pi$ ) as a function of  $J_y$  at  $J_x = 0.6$  for different phases of the model, where  $Q_x$  is the pitch angle for the X-spiral phase varying along  $x$ -direction. The pink line is the value of pitch angles calculated using Eq. 3. In both plots we have used  $12 \times 4$  system size.

dotted line with circles whereas the classical results are shown as solid line as shown in Fig. 6(b). The calculated values of  $Q_x$  suggest that it is zero below the dimer line and increase rapidly with  $J_y$  and reaches to  $\pi$  for  $J_y \sim 1.0$ . In the stripe ( $\pi, 0$ ) phase the  $Q_x$  is  $\pi$ , whereas it is zero in the stripe ( $0, \pi$ ) phase. These systems have correlation length  $\xi \approx 4$  lattice units, therefore, there is an error in calculating the  $Q_x$  and it is represented by error bars. The system remains invariant by exchanging the  $J_y$  to  $J_x$  interaction, therefore  $Q_x - J_y$  and  $Q_y - J_x$  curves have the same nature as shown in  $Q_x - J_y$  curve.

#### IV. SUMMARY AND CONCLUSION

In this work, we construct a new quantum phase diagram of ferromagnetically coupled  $S = 1/2$  on the SSL. Exchange couplings along width  $J_y$  and length  $J_x$  are ferromagnetic, whereas, the exchange couplings along diagonal bonds  $J$  are antiferromagnetic. The quantum phase diagram of the SSM in Eq. 1 consists of six phases and the phase boundaries are calculated based on spin-spin correlation and the gs energies obtained using the ED and the DMRG methods. Our numerical calculations are

done upto  $12 \times 8$  lattices and we have used PBC along the width and OBC along length. Almost everywhere in the phase space the order is short range and correlation length  $\xi$  is less than equal to 4 lattice unit, therefore, most of our calculations give reliable results for the two dimensional lattice of this model. The six phases in the phase diagrams are: (I) stripe  $(0, \pi)$ , (II) stripe  $(\pi, 0)$ , (III) perfect dimer, (IV)  $X$ -spiral, (V)  $Y$ -spiral and (VI) ferromagnetic state. Our analysis also confirms the existence of spiral phases in this model for moderate FM couplings strength.

Our DMRG results are very different from the Schwinger-Boson mean-field theory in Ref. [54]. Although quantum phases predicted by mean-field theory are also found in the DMRG results but phases boundaries are quite different. DMRG calculations suggest that perfect dimer singlet phase is confined to only on  $J_x = J_y$  line, whereas the mean-field calculation suggests a large area of this regime. Our result is consistent with the ED results<sup>54</sup>. Our results also suggest that second nearest neighbour correlation increases continuously with  $|J_x - J_y|$  i.e. short range but finite correlation exists in the neighbourhood of dimer line except the  $J_x = J_y$  line where only diagonal correlations are non zero. The mean-field results suggest the non-collinear spin wave along the  $x$ - and  $y$ -direction but ED does not confirm the results<sup>54</sup>. DMRG results confirm both types of the non-collinear phases. The mean-field pitch angle variation is small compared to the DMRG value in most parts of the parameter regime.

Tassel *et al.* suggested that  $(\text{CuCl})\text{LaNb}_2\text{O}_7$  has fer-

romagnetic  $J_y/J \sim 0.39$  and  $J_x/J \sim 0.38$ <sup>53</sup> and therefore, we expect this system should behave like dimer as it is on  $J_x = J_y$  dimer singlet line. Although, Tsirlin *et al.* shows different exchange interactions using the two types of DFT calculations<sup>46</sup>. However, the data of inelastic neutron scattering (INS) on powder samples shows that the dynamical structure factor has  $S(Q, \omega)$  maxima around  $Q \sim 0.5\text{\AA}$ , i.e. it is in a non-collinear regime. In our opinion this material is in the neighbourhood of dimer phase but detailed theoretical investigation is required to understand the spin configuration in the system.

In conclusion, we numerically studied the SSM and constructed a new quantum phase diagram using the DMRG method. We have also calculated the correlation function and pitch angle which can be directly connected to INS data. The phase boundaries calculated from DMRG results are different from that of mean-field and ED calculations. We hope that interesting quantum phases in real material like  $(\text{CuCl})\text{LaNb}_2\text{O}_7$  and others<sup>53,63–65</sup> can be revisited in light of this study. The short-range spiral phase in the frustrated regime of the model can be manipulated by external probe like a magnetic field, doping, etc. and might lead to many interesting phases. The effect of field on phase diagram of the model in Eq. 1 is still an open problem.

#### ACKNOWLEDGMENTS

MK thanks SERB for financial support through grant sanction number CRG/2020/000754. MC thanks DST-INSPIRE for financial support and also thanks S K Saha for fruitful discussions.

\* c.monalisa1993@bose.res.in

† santanu1720@bose.res.in

‡ manoranjan.kumar@bose.res.in

<sup>1</sup> S. White, R. Noack, and D. Scalapino, *Physical Review Letters* **73**, 886 (1994).

<sup>2</sup> M. Kumar, A. Parvej, and Z. G. Soos, *Journal of Physics: Condensed Matter* **27**, 316001 (2015).

<sup>3</sup> Y. Zhou, K. Kanoda, and T.-K. Ng, *Reviews of Modern Physics* **89**, 025003 (2017).

<sup>4</sup> L. Savary and L. Balents, *Reports on Progress in Physics* **80**, 016502 (2016).

<sup>5</sup> L. Balents, *Nature* **464**, 199 (2010).

<sup>6</sup> P. A. Lee, *Science* **321**, 1306 (2008).

<sup>7</sup> T.-H. Han, J. S. Helton, S. Chu, D. G. Nocera, J. A. Rodriguez-Rivera, C. Broholm, and Y. S. Lee, *Nature* **492**, 406 (2012).

<sup>8</sup> M. Fu, T. Imai, T.-H. Han, and Y. S. Lee, *Science* **350**, 655 (2015).

<sup>9</sup> S. Dutton, M. Kumar, M. Mourigal, Z. G. Soos, J.-J. Wen, C. L. Broholm, N. H. Andersen, Q. Huang, M. Zbiri, R. Toft-Petersen, *et al.*, *Physical Review Letters* **108**, 187206 (2012).

<sup>10</sup> M. Mourigal, M. Enderle, B. Fåk, R. Kremer, J. Law, A. Schneidewind, A. Hiess, and A. Prokofiev, *Physical*

*Review Letters* **109**, 027203 (2012).

<sup>11</sup> M. Hase, H. Kuroe, K. Ozawa, O. Suzuki, H. Kitazawa, G. Kido, and T. Sekine, *Physical Review B* **70**, 104426 (2004).

<sup>12</sup> A. Yagi, K. Matsui, T. Goto, M. Hase, and T. Sasaki, in *Journal of Physics: Conference Series*, Vol. 828 (IOP Publishing, 2017) p. 012016.

<sup>13</sup> A. W. Sandvik, E. Dagotto, and D. J. Scalapino, *Physical Review B* **53**, R2934 (1996).

<sup>14</sup> D. Johnston, J. Johnson, D. Goshorn, and A. Jacobson, *Physical Review B* **35**, 219 (1987).

<sup>15</sup> E. Dagotto and T. Rice, *Science* **271**, 618 (1996).

<sup>16</sup> M. P. Shores, E. A. Nytko, B. M. Bartlett, and D. G. Nocera, *Journal of the American Chemical Society* **127**, 13462 (2005).

<sup>17</sup> J. Helton, K. Matan, M. Shores, E. Nytko, B. Bartlett, Y. Yoshida, Y. Takano, A. Suslov, Y. Qiu, J.-H. Chung, *et al.*, *Physical Review Letters* **98**, 107204 (2007).

<sup>18</sup> A. Banerjee, C. Bridges, J.-Q. Yan, A. Aczel, L. Li, M. Stone, G. Granroth, M. Lumsden, Y. Yiu, J. Knolle, *et al.*, *Nature Materials* **15**, 733 (2016).

<sup>19</sup> C. Broholm, R. Cava, S. Kivelson, D. Nocera, M. Norman, and T. Senthil, *Science* **367** (2020).

- <sup>20</sup> B. Lake, D. A. Tennant, C. D. Frost, and S. E. Nagler, *Nature Materials* **4**, 329 (2005).
- <sup>21</sup> M. Norman, *Reviews of Modern Physics* **88**, 041002 (2016).
- <sup>22</sup> H. Takagi, T. Takayama, G. Jackeli, G. Khaliullin, and S. E. Nagler, *Nature Reviews Physics* **1**, 264 (2019).
- <sup>23</sup> J.-B. Fouet, F. Mila, D. Clarke, H. Youk, O. Tchernyshyov, P. Fendley, and R. Noack, *Physical Review B* **73**, 214405 (2006).
- <sup>24</sup> N. Shannon, T. Momoi, and P. Sindzingre, *Physical Review Letters* **96**, 027213 (2006).
- <sup>25</sup> T. Hikihara, L. Kecke, T. Momoi, and A. Furusaki, *Physical Review B* **78**, 144404 (2008).
- <sup>26</sup> A. Leonov and M. Mostovoy, *Nature Communications* **6**, 1 (2015).
- <sup>27</sup> T. Momoi and K. Totsuka, *Physical Review B* **62**, 15067 (2000).
- <sup>28</sup> J. Schulenburg, A. Honecker, J. Schnack, J. Richter, and H.-J. Schmidt, *Physical Review Letters* **88**, 167207 (2002).
- <sup>29</sup> C. K. Majumdar and D. K. Ghosh, *Journal of Mathematical Physics* **10**, 1388 (1969).
- <sup>30</sup> R. Chitra, S. Pati, H. Krishnamurthy, D. Sen, and S. Ramasesha, *Physical Review B* **52**, 6581 (1995).
- <sup>31</sup> Z. G. Soos, A. Parvej, and M. Kumar, *Journal of Physics: Condensed Matter* **28**, 175603 (2016).
- <sup>32</sup> B. S. Shastry and B. Sutherland, *Physica B+ C* **108**, 1069 (1981).
- <sup>33</sup> S. Chakravarty, B. I. Halperin, and D. R. Nelson, *Physical Review B* **39**, 2344 (1989).
- <sup>34</sup> E. Dagotto and A. Moreo, *Physical Review Letters* **63**, 2148 (1989).
- <sup>35</sup> J. Sirker, Z. Weihong, O. Sushkov, and J. Oitmaa, *Physical Review B* **73**, 184420 (2006).
- <sup>36</sup> S. Kundu, A. Shahee, A. Chakraborty, K. Ranjith, B. Koo, J. Sichelschmidt, M. T. Telling, P. Biswas, M. Baenitz, I. Dasgupta, *et al.*, *Physical Review Letters* **125**, 267202 (2020).
- <sup>37</sup> E. Manousakis, *Reviews of Modern Physics* **63**, 1 (1991).
- <sup>38</sup> Y. Shirata, H. Tanaka, A. Matsuo, and K. Kindo, *Physical Review Letters* **108**, 057205 (2012).
- <sup>39</sup> H. Kageyama, K. Yoshimura, R. Stern, N. Mushnikov, K. Onizuka, M. Kato, K. Kosuge, C. Slichter, T. Goto, and Y. Ueda, *Physical Review Letters* **82**, 3168 (1999).
- <sup>40</sup> M. Zayed, C. Rüegg, A. Läuchli, C. Panagopoulos, S. Saxena, M. Ellerby, D. McMorrow, T. Strässle, S. Klotz, G. Hamel, *et al.*, *Nature Physics* **13**, 962 (2017).
- <sup>41</sup> J. Y. Lee, Y.-Z. You, S. Sachdev, and A. Vishwanath, *Physical Review X* **9**, 041037 (2019).
- <sup>42</sup> N. D. Mermin and H. Wagner, *Physical Review Letters* **17**, 1133 (1966).
- <sup>43</sup> P. Corboz and F. Mila, *Physical Review B* **87**, 115144 (2013).
- <sup>44</sup> J. Yang, A. W. Sandvik, and L. Wang, *arXiv preprint arXiv:2104.08887* (2021).
- <sup>45</sup> D. C. Ronquillo and M. R. Peterson, *Physical Review B* **90**, 201108 (2014).
- <sup>46</sup> A. A. Tsirlin, A. M. Abakumov, C. Ritter, and H. Rosner, *Physical Review B* **86**, 064440 (2012).
- <sup>47</sup> H. Kageyama, T. Kitano, N. Oba, M. Nishi, S. Nagai, K. Hirota, L. Viciu, W. JB, J. Yasuda, Y. Baba, *et al.*, *Journal of the Physical Society of Japan* **74**, 1702 (2005).
- <sup>48</sup> H. Kageyama, J. Yasuda, T. Kitano, K. Totsuka, Y. Narumi, M. Hagiwara, K. Kindo, Y. Baba, N. Oba, Y. Ajiro, *et al.*, *Journal of the Physical Society of Japan* **74**, 3155 (2005).
- <sup>49</sup> A. Kitada, Z. Hiroi, Y. Tsujimoto, T. Kitano, H. Kageyama, Y. Ajiro, and K. Yoshimura, *Journal of the Physical Society of Japan* **76**, 093706 (2007).
- <sup>50</sup> M. Yoshida, N. Ogata, M. Takigawa, J.-i. Yamaura, M. Ichihara, T. Kitano, H. Kageyama, Y. Ajiro, and K. Yoshimura, *Journal of the Physical Society of Japan* **76**, 104703 (2007).
- <sup>51</sup> N. Oba, H. Kageyama, T. Kitano, J. Yasuda, Y. Baba, M. Nishi, K. Hirota, Y. Narumi, M. Hagiwara, K. Kindo, *et al.*, *Journal of the Physical Society of Japan* **75**, 113601 (2006).
- <sup>52</sup> Y. Tsujimoto, Y. Baba, N. Oba, H. Kageyama, T. Fukui, Y. Narumi, K. Kindo, T. Saito, M. Takano, Y. Ajiro, *et al.*, *Journal of the Physical Society of Japan* **76**, 063711 (2007).
- <sup>53</sup> C. Tassel, J. Kang, C. Lee, O. Hernandez, Y. Qiu, W. Paulus, E. Collet, B. Lake, T. Guidi, M.-H. Whangbo, *et al.*, *Physical Review Letters* **105**, 167205 (2010).
- <sup>54</sup> S. Furukawa, T. Dodds, and Y. B. Kim, *Physical Review B* **84**, 054432 (2011).
- <sup>55</sup> S. R. White, *Physical Review Letters* **69**, 2863 (1992).
- <sup>56</sup> S. R. White, *Physical Review B* **48**, 10345 (1993).
- <sup>57</sup> U. Schollwöck, *Reviews of Modern Physics* **77**, 259 (2005).
- <sup>58</sup> K. A. Hallberg, *Advances in Physics* **55**, 477 (2006).
- <sup>59</sup> M. Kumar, Z. G. Soos, D. Sen, and S. Ramasesha, *Physical Review B* **81**, 104406 (2010).
- <sup>60</sup> S. Furukawa, M. Sato, S. Onoda, and A. Furusaki, *Physical Review B* **86**, 094417 (2012).
- <sup>61</sup> A. Parvej and M. Kumar, *Physical Review B* **96**, 054413 (2017).
- <sup>62</sup> D. Maiti and M. Kumar, *Physical Review B* **100**, 245118 (2019).
- <sup>63</sup> Y. Uemura, A. Aczel, Y. Ajiro, J. Carlo, T. Goko, D. Goldfeld, A. Kitada, G. Luke, G. MacDougall, I. Mihailescu, *et al.*, *Physical Review B* **80**, 174408 (2009).
- <sup>64</sup> A. Kitada, Y. Tsujimoto, H. Kageyama, Y. Ajiro, M. Nishi, Y. Narumi, K. Kindo, M. Ichihara, Y. Ueda, Y. Uemura, *et al.*, *Physical Review B* **80**, 174409 (2009).
- <sup>65</sup> Y. Tsujimoto, A. Kitada, H. Kageyama, M. Nishi, Y. Narumi, K. Kindo, Y. Kiuchi, Y. Ueda, Y. J. Uemura, Y. Ajiro, *et al.*, *Journal of the Physical Society of Japan* **79**, 014709 (2009).

## V. APPENDIX

$L_x \times L_y$	$J_x$	$J_y$	$m$	$\epsilon_{gs}$
$12 \times 4$	0.6	0.21	256	-0.357791
			512	-0.357795
			900	-0.357798
$12 \times 8$	0.6	1.0	256	-0.36989
			512	-0.36987
			700	-0.36984

TABLE I. The table shows the gs energy per site ( $\epsilon_{gs}$ ) calculated for various bond dimensions ( $m$ ). For the system size  $12 \times 4$  gs energy calculated for  $J_x = 0.6$  and  $J_y = 0.21$ , whereas for  $12 \times 8$  system size, it is calculated for  $J_x = 0.6$  and  $J_y = 1.0$ .

direction	$r$	$m = 256$	$m = 512$	$m = 900$
length	1	0.02154	0.02153	0.02152
	2	0.00652	0.00651	0.00650
	3	0.00182	0.00182	0.00178
	4	0.00056	0.00056	0.00053
	5	0.00015	0.00015	0.00014
width	1	-0.02269	-0.02269	-0.02267
	2	0.01006	0.01006	0.01008

TABLE II. The table shows spin-spin correlation  $\langle S_i^z S_{i+r}^z \rangle$  calculated for various bond dimensions ( $m$ ) for  $12 \times 4$  system size. The correlation calculated along length and width for  $J_x = 0.6$  and  $J_y = 0.21$ , where the last three columns are the correlation values for the corresponding  $m$ .

direction	$r$	$m = 256$	$m = 512$	$m = 700$
length	1	-0.02095	-0.02097	-0.02088
	2	0.00354	0.00338	0.00328
	3	-0.00037	-0.00032	-0.00030
	4	0.000058	0.000050	0.000042
	5	-0.000006	-0.000019	-0.000004
	6	-0.000001	0.000033	0.000001
width	1	0.021093	0.021144	0.021042
	2	0.008490	0.008516	0.008512
	3	0.002574	0.002553	0.002526
	4	0.001771	0.001719	0.001769

TABLE III. The table shows spin-spin correlation  $\langle S_i^z S_{i+r}^z \rangle$  calculated for various bond dimensions ( $m$ ) for  $12 \times 8$  system size. The correlation calculated along length and width for  $J_x = 0.6$  and  $J_y = 1.0$ , where the last three columns are the correlation values for the corresponding  $m$ .